Review of Scientific Instruments ARTICLE scitation.org/journal/rsi

Development of Faraday rotation measurements on Keda Reconnection eXperiment (KRX) device

Cite as: Rev. Sci. Instrum. 92, 053516 (2021); doi: 10.1063/5.0043882
Submitted: 12 January 2021 • Accepted: 17 April 2021 •
Published Online: 6 May 2021

D. K. Liu,[1] W. X. Ding,[1,2,a)] W. Z. Mao,[2] Q. F. Zhang,[1] F. B. Fan,[1] L. L. Sang,[1] Q. M. Lu,[1] and J. L. Xie[1,2]

AFFILIATIONS

[1] CAS Key Lab of Geoscience Environment, School of Earth and Space Sciences, University of Science and Technology of China, Hefei 230026, China

[2] Department of Plasma Physics and Nuclear Engineering, University of Science and Technology of China, Hefei 230026, China

Note: Paper published as part of the Special Topic on Proceedings of the 23rd Topical Conference on High-Temperature Plasma Diagnostics.

[a)] **Author to whom correspondence should be addressed:** wxding@ustc.edu.cn

ABSTRACT

The Faraday-effect based polarimeter and interferometer are developed for non-perturbation magnetic field and density measurements on the Keda Reconnection eXperiment (KRX) device. The magnetic reconnection is externally driven by a pair of parallel current plates. To design this instrument and provide an alternative way to facilitate theory–experiment comparisons via forward modeling of the diagnostics process with full plasma dynamics given by simulation, we develop a synthetic diagnostics based on 2D photonic integrated circuit simulation for magnetic reconnection on the KRX. The view-line geometry is optimized and wavelengths (1 mm) of the polarimeter and interferometer are selected to ensure the sensitivity of measurement on the KRX. We have simulated magnetic reconnection on the x-line (x–z plane) with horizontal viewing and vertical viewing for line of sight measurements. It is found that the current sheet width and indicator of magnetic reconnection can be inferred directly from the dynamics of Faraday rotation even with the line-integrated character of polarimeter–interferometer diagnostics.

I. INTRODUCTION

The Keda Reconnection eXperiment (KRX) device is under development to investigate the fundamental physics of magnetic reconnection. As shown in Fig. 1, the KRX is a linear device and the stainless steel vacuum chamber is 10 m long with a diameter of 3 m. The magnetic reconnection is driven by a pair of parallel current plates with multiple slots that allow the probing beam to pass through. Each discharge is 10 ms. The red arrow represents the vertical viewing of the probing beam, and the blue arrow represents the horizontal viewing of the probing beam in our polarimeter–interferometer systems. The experimental region is ~2.5 × 1 m^2, and the reconnection magnetic field is 0–500 G. The plasma density is 10^{16}–10^{19} m^{-3}, the electron inertial length (c/ω_{pe}) is 1–10 mm, and the ion inertial length (c/ω_{pi}) is 10–100 cm. The experimental area contains 10 × 5 ion inertial lengths, which allows the KRX to study the electron scale reconnection together with ion scale reconnection under an approximately collisionless condition.

As basic methods to measure magnetic field and plasma parameters, the probe diagnostics (magnetic probes, electric field probes, Langmuir probes, and Mach probes) are widely used in the magnetic reconnection experiments, such as MRX,[1,2] LAPD,[3] and TREX.[4] However, the measurement of the narrow current sheet remains a challenge in the laboratory plasma since probes may disturb plasmas. For non-perturbation measurement, the Faraday-effect based polarimeter/interferometer diagnostics is now considered as one of the reliable methods to measure the magnetic field, current density, and electron density in the tokamak plasma.[5,6] Motivated by the needs of the magnetic reconnection diagnostics on the KRX device, the Faraday effect based polarimeter and interferometer are being developed for non-perturbation electron density and current density profile diagnostics for the KRX under construction.

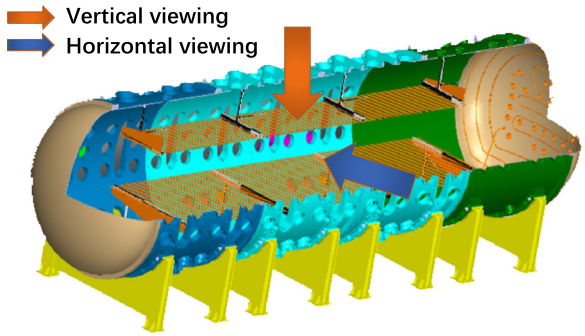

FIG. 1. The schematic view of the Keda Reconnection eXperiment device. The vertical view (red arrow) and the horizontal view (blue arrow) of the probing beam in the polarimeter–interferometer system are given.

Before designing the polarimeter and interferometer for the KRX, a two-dimensional particle-in-cell simulation model is used to investigate the Faraday effect during the evolution of collisionless reconnection and determine the proper wavelength of the probing beam, optical paths, and the best of line of sight to reveal reconnection physics. The simulation model and results are presented in Sec. II and Sec. III, respectively, and the bench test results are discussed in Sec. IV.

II. SIMULATION MODEL

In order to investigate the Faraday effect in the case of magnetic reconnection, the 2D photonic integrated circuit (PIC) simulations are performed in the (x, z) plane. In the PIC simulation, the electromagnetic fields are defined on the grids and updated by solving the Maxwell equations with a full explicit algorithm, and both ions and electrons are advanced by integrating the Newton–Lorentz equations.[7] The initial configuration is a 1D Harris sheet equilibrium in the (x, z) plane with an initial magnetic field $B_0(z) = B_0 \tanh(z/\delta)e_x$, where B_0 is the asymptotical magnetic field and $\delta$is the half-width of the current sheet, and the corresponding particle number density is given by $n(z) = n_b + n_0 \operatorname{sech}^2(z/\delta)$, where n_b is the background density and n_0 is the number density in the center of the current. Both ions and electrons initially have the Maxwellian velocity distribution with a drift speed in the y direction, and the drift speed satisfies the equation $V_{i0}/V_{e0} = -T_{i0}/T_{e0}$, where V_{i0} (V_{e0}) and T_{i0} (T_{e0}) are the initial drift speed and temperature of ions (electrons), respectively. The size of the simulation domain is $L_x \times L_z = 50d_i \times 50d_i$, where $d_i = c/\omega_{pi}$ is the ion inertial length and c is the speed of light. We employ an $N_x \times N_z = 1000 \times 1000$ grid system in our simulations, whose spatial resolution is $\Delta x = \Delta z = 0.05d_i$ and time resolution is $\Omega_i \Delta t = 0.001$ (where $\Omega_i = eB_0/m_i$ is the ion gyrofrequency). We set $T_{i0}/T_{e0} = 4$ and $n_b = 0.2n_0$. The CS initial width is $\delta = 0.5d_i$, the ion-to-electron mass ratio is 100, and $c = 15v_A$. The periodic boundary conditions are employed in the x direction, while the ideal conducting boundary conditions for the electromagnetic fields are employed in the z direction. An initial flux perturbation is introduced to make the system enter the nonlinear stage quickly.

III. SIMULATION RESULTS

In the KRX, the experimental region contains 10×5 ion inertial lengths, and we choose the same region in the simulation region with negligible boundary conditions to analyze the Faraday effect using synthetic diagnostics.

Figure 2(a) plots the contour of the Hall magnetic field at $\Omega_i t$ = 10, 15, 20, and 25, respectively. With the proceeding of the reconnection, the out-of-plane magnetic field grows fast and the maximum of the out-of-plane magnetic field is ~0.25 B_0, and the trigger of the reconnection is approximately at $\Omega_i t = 15$. Figure 2(b) presents the evolution of the out-of-plane current sheet at $\Omega_i t = 10, 15, 20,$ and 25. It can be seen from the picture that the current sheet becomes thinner with the proceeding of the reconnection.

As the probing beam passes through the plasma, the phase shift of line-integrated density measurement from the interferometer can be described as $\phi = C_I \lambda \int n_e dl$, where $C_I = 2.82 \times 10^{-15}$, n_e is the electron density, λ is the wavelength, and l is the integrated path length along the probing beam. The Faraday rotation angle from the polarimeter can be expressed as $\theta_f = C_f \lambda^2 \int n_e B_\parallel dl$, where $C_f = 2.62 \times 10^{-13}$ and $B_\parallel$ is part of the magnetic field that is parallel to the propagating probing beam.[6] In this condition, we can calculate the integration of the electron density n_e and the magnetic field B_x along the probing beam in the x direction. B_x is normalized by B_0, n_e is normalized by n_0, and l is normalized by d_i. The Faraday rotation angle and line-integrated density are quantities to be measured in experiments. As shown in Fig. 3(a), we scan the simulation region along the z direction from $z = -2.5d_i$ to $z = 2.5d_i$, and the integration path is from $x = -5d_i$ to $x = 5d_i$ of the simulation region (horizontal view). Figure 3(b) gives the horizontal view of the time evolution of the Faraday rotation of line-integrated magnetic field and electron

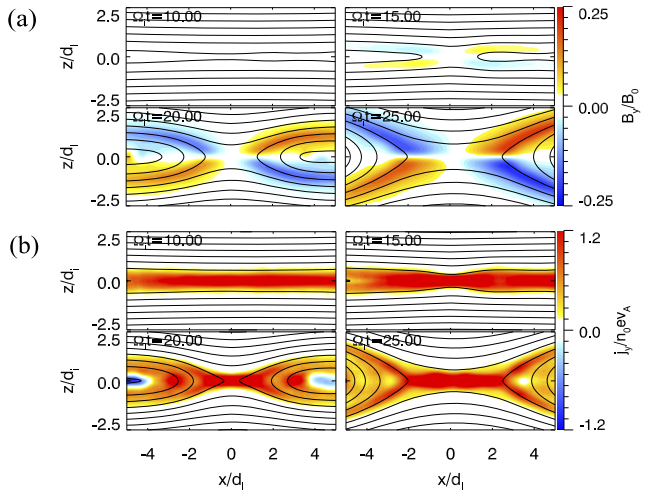

FIG. 2. The PIC simulation results. (a) The evolution of the out-of-plane magnetic field B_y at $\Omega_i t$ = 10, 15, 20, and 25 from $x = -5d_i$ to $x = 5d_i$ around the reconnection site. The solid lines represent the in-plane magnetic field for reference. (b) The evolution of the total out-of-plane current density at $\Omega_i t$ = 10, 15, 20, and 25 from $x = -5d_i$ to $x = 5d_i$. The in-plane magnetic field (black lines) is also plotted for reference.

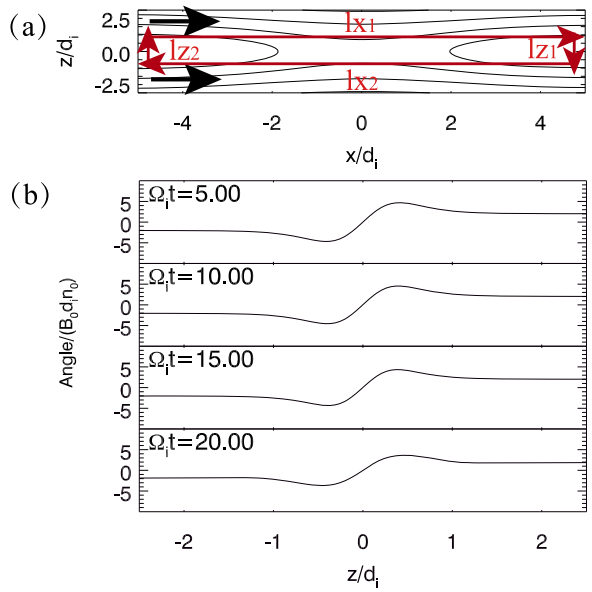

FIG. 3. Simulation results. (a) The contour of the magnetic field. The black arrows represent the direction of the probing beam. The red arrows represent the reconnection current sheet profile. (b) The horizontal viewing of the time evolution of the Faraday rotation of the line-integrated magnetic field and electron density $\int n_e B_\parallel dl$ in the PIC simulation along the parallel probing beam simultaneously at $\Omega_i t$ = 5, 10, 15, and 20. The angle of the Faraday effect is in units of $B_0 d_i n_0$.

density $\int n_e B_\parallel dl$ in the PIC simulation along the parallel probing beam direction simultaneously at $\Omega_i t$ = 5, 10, 15, and 20. It can be seen from the figure that the Faraday rotation angle has a positive maximum value and negative minimum value due to the opposite magnetic field lines across the reconnection layer.

When reconnection occurs ($\Omega_i t$ = 15), the Faraday rotation angle becomes smaller, implying flux conversion. Moreover, according to the Ampere loop theorem $\oint Bdl = \mu_0 I$, the current density j_y can be derived through the Faraday rotation effect, which leads to

$$\oint Bdl = \mu_0 I, \tag{1}$$

$$\begin{aligned}\oint Bdl &= \int B_x dl_{x1} + \int B_z dl_{z1} + \int B_x dl_{x2} + \int B_z dl_{z2} \\ &\approx \int B_x dl_{x1} + \int B_x dl_{x2} \\ &\approx \frac{\theta_{f\max} - \theta_{f\min}}{n_e},\end{aligned} \tag{2}$$

$$j_y = \frac{\theta_{f\max} - \theta_{f\min}}{n_e \mu_0 S}, \tag{3}$$

$$S = l_{x1} \cdot l_{z1} = l_{x2} \cdot l_{z2}. \tag{4}$$

In Eqs. (2) and (4), l_{x1} and l_{x2} are the lengths of the experimental region. l_{z1} and l_{z2} are the distances between the maximum value of the Faraday rotation angle and the minimum value of the Faraday rotation angle, which represent the width of the current layer, as shown in Fig. 3(a). n_e is the average electron density. In Fig. 4, the black solid line represents the evolution of the mean current density around the X line. The diamond points represent the derived current density by Eq. (3). It can be seen from the figure that the calculated current density basically agrees well with the derived current density using the polarimetry loop, so the Faraday effect can be directly used to measure the current layer in the magnetic reconnection process.

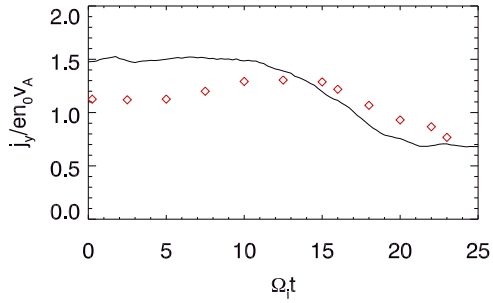

FIG. 4. The time evolution of the average out-of-plane current density of the current layer (black line) and the derived current density from the Faraday rotation angle (the diamond line) at $\Omega_i t$ = 0–25.

An extended current layer can be generated in the middle region, and a strong magnetic field B_z will be generated during magnetic reconnection. Faraday rotation measurement can be used to determine the trigger of the reconnection since it directly measures the change of magnetic topology. Figure 5(b) presents vertical viewing of integration $\int n_e B_\parallel dl$ of the reconnection at $\Omega_i t$ = 10, 15, 20, and 25. It can be seen from the plot that the angle of the Faraday effect becomes larger with the proceeding of the

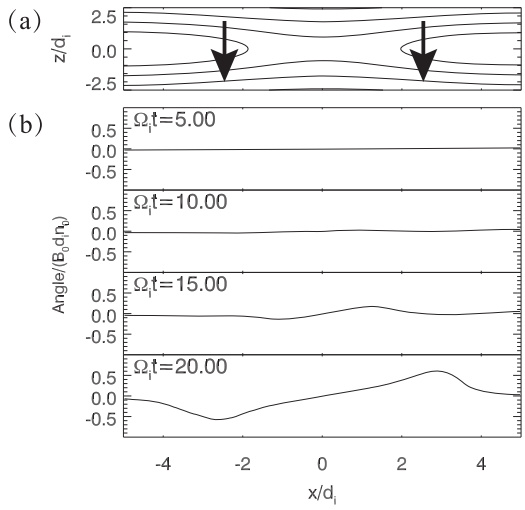

FIG. 5. Simulation results. (a) The contour of the magnetic field. The black arrows represent direction of the probing beam. (b) The vertical viewing of time evolution of the Faraday rotation of line-integrated magnetic field and density of electrons $\int n_e B_\parallel dl$ in the PIC simulation along the vertical probing beam simultaneously at $\Omega_i t$ = 5, 10, 15, and 20. The angle of the Faraday effect is in units of $B_0 d_i n_0$.

reconnection, which can be used to investigate the onset of magnetic reconnection.

In order to obtain sufficient Faraday rotation angle and plasma phase shift to be measured using a polarimeter and an interferometer, respectively, an appropriate wavelength of the probing beam should be selected. With a 1 mm wavelength microwave source, the simulation shows that the phase difference measured by the interferometer on the KRX is tens of degrees, and the Faraday rotation angle measured using the polarimeter is less than 1° (not presented), which can meet the measurement requirements. All of the results show that the polarimeter–interferometer diagnostics remains as an essential tool for us to study reconnection physics in the laboratory.

IV. OPTICAL PATH AND BENCH TEST OF INTERFEROMETER

The polarimeter/interferometer diagnostics is under development for magnetic field and electron density measurement on the KRX device. In order to improve the accuracy of the polarimeter/interferometer, the bench test is conducted before installation on the KRX.

As described in detail in Fig. 6, the typical three-wave optical geometric configuration of the interferometer system has been used in the bench test,[5] but one of the waves among three (ω_1, ω_2, and ω_3) has not been tested, and we tested the interferometer using ω_1 and ω_2 only in the text.[8,9] The two laser beams are used as the reference beam and the probing beam in the interferometer system. The frequency adjustable 320 GHz solid-state VDI microwave sources are used in the system. The frequency range can be adjusted from 316 to 324 GHz with 15 mW output power. Low noise and high responsivity (~1300 V/W) WR2.8FM VDI planar-diode mixers are used for detectors. The intermediate frequency (IF) output is 1–40 MHz. The interferometer system is firstly aligned by He–Ne lasers,[10] then the signal (probing) beam and the reference beam both are divided by mesh beam splitters (50% beam, LPI = 70) and are mixed with local oscillators to generate a heterodyne system. The IF is set to be ~1 MHz. We use the National Instruments A/D card (model PXIe-5105) with fast time response and high phase resolution sensitivity as our data acquisition.

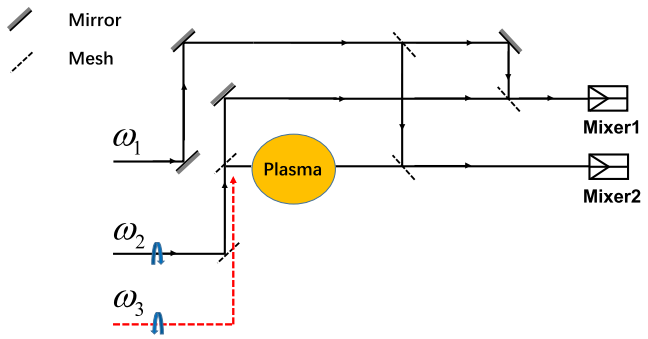

FIG. 6. The typical three-wave optical geometric configuration of the interferometer. The broken line in red will be installed.

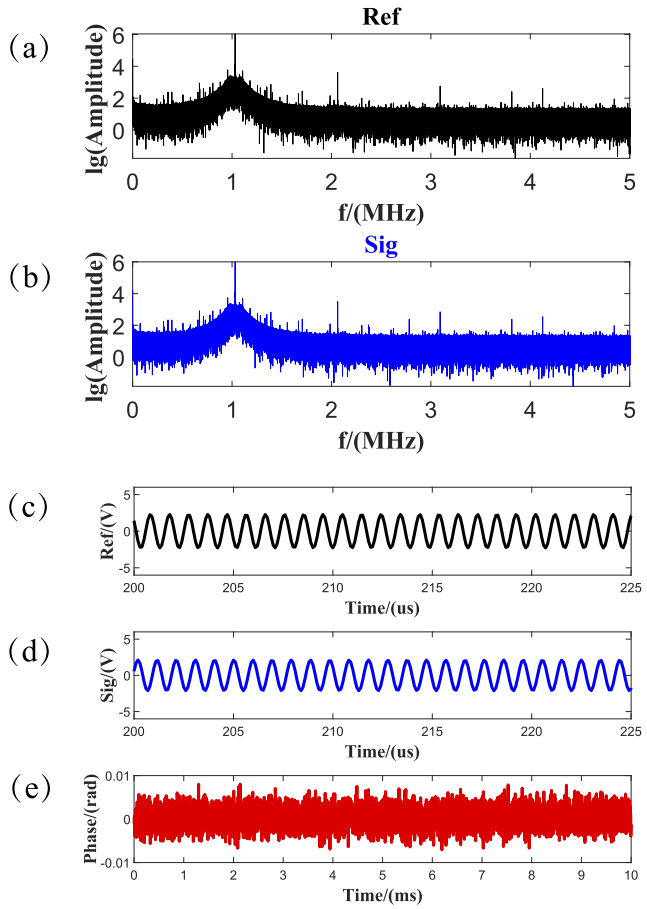

FIG. 7. The typical signal spectrum of the intermediate frequency (IF) signal of (a) the reference beam and (b) the signal beam. Time series of IF with a bandwidth of 300 kHz of (c) the reference beam and (d) the signal beam. (e) The phase difference noise between the reference beam and the signal beam.

As shown in Figs. 7(a) and 7(b), in the frequency spectrum, the IF signal is ~1 MHz with its harmonics generated by the mixer itself. These harmonics can be reduced by the reduction of signal amplitude. Figures 7(c) and 7(d) show the reference signal and probing signal both with a digital band pass filter (0.3 MHz). The phase difference noise between probing and reference signals is plotted in Fig. 7(e).

We also introduce an ω_3 probing beam collinear with ω_2 to investigate the polarimeter system phase. Since there are no birefringence materials in the probing beam path, phase noise is essentially equivalent to the phase noise of a polarimeter. The system phase noise varies with the bandwidth as expected. As shown in Fig. 8, the phase noise increases slightly while the bandwidth is increased, which indicates that the white noise level is relatively low. The lowest noise level for a polarimeter is ~0.15°. For an interferometer, the minimum noise is 1.2°, which is larger than that of a polarimeter as usual. Compared with tens of degrees of phase shift expected to be measured on the KRX, the noise is low enough and the system can be used for interferometer measurement on the KRX.

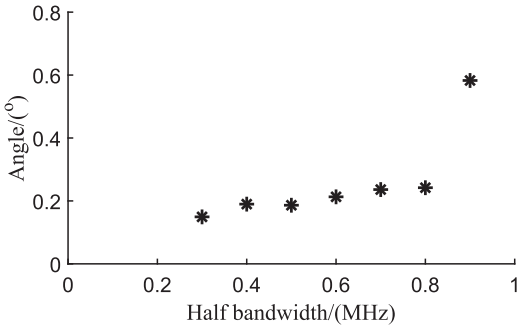

FIG. 8. The relationship of the filter half bandwidth and the system noise angle.

V. CONCLUSION AND DISCUSSION

Synthetic diagnostics from PIC simulation indicates that the Faraday rotation measurement can be used directly to infer the reconnection current sheet width with a very good approximation. In addition to measuring the electron density and magnetic field, the trigger of magnetic reconnection can also be inferred from the dynamics of Faraday rotation with line-intergrated polarimeter–interferometer diagnostics. We select the 320 GHz frequency of the polarimeter and interferometer system to ensure the sensitivity of the measurement on the KRX. The noise of the interferometer is under optimization in bench. A further improved accurate low noise polarimeter system is expected to serve for the measurement of the Faraday rotation angle on the KRX, which is under construction.

ACKNOWLEDGMENTS

This material was based upon work supported by CNSF (Grant Nos. 41527906 and 11975231).

DATA AVAILABILITY

The data that support the findings of this study are available from the corresponding author upon reasonable request.

REFERENCES

[1]H. Ji, M. Yamada, S. Hsu, and R. Kulsrud, Phys. Rev. Lett. **80**(15), 3256–3259 (1998).
[2]Y. Ren, M. Yamada, S. Gerhardt, H. T. Ji, R. Kulsrud, and A. Kuritsyn, Phys. Rev. Lett. **95**(5), 055003 (2005).
[3]W. Gekelman, P. Pribyl, Z. Lucky, S. W. Tang, J. Han, and Y. Qian, J. Plasma Phys. **86**(3), 925860301 (2020).
[4]J. Olson, J. Egedal, S. Greess, R. Myers, M. Clark, D. Endrizzi, K. Flanagan, J. Milhone, E. Peterson, J. Wallace, D. Weisberg, and C. B. Forest, Phys. Rev. Lett. **116**(25), 255001 (2016).
[5]W. X. Ding, D. L. Brower, W. F. Bergerson, and L. Lin, Rev. Sci. Instrum. **81**(10), 10D508 (2010).
[6]W. X. Ding, D. L. Brower, S. D. Terry, D. Craig, S. C. Prager, J. S. Sarff, and J. C. Wright, Phys. Rev. Lett. **90**(3), 035002 (2003).
[7]Q. M. Lu, C. Huang, J. L. Xie, R. S. Wang, M. Y. Wu, A. Vaivads, and S. Wang, J. Geophys. Res. **115**, A11208, https://doi.org/10.1029/2010ja015713 (2010).
[8]D. Véron, Opt. Commun. **10**(1), 95–98 (1974).
[9]D. Veron, in *Infrared and Millimeter Waves*, edited by K. J. Button (Academic, New York, 1979), Vol. 2, pp. 67–135.
[10]H. Q. Liu, Y. X. Jie, W. X. Ding, D. L. Brower, Z. Y. Zou, W. M. Li, Z. X. Wang, J. P. Qian, Y. Yang, L. Zeng, T. Lan, X. C. Wei, G. S. Li, L. Q. Hu, and B. N. Wan, Rev. Sci. Instrum. **85**(11), 11D405 (2014).